Segmentation and wake removal of seafaring vessels in optical satellite images

Henri Bouma [*], Rob J. Dekker, Robin M. Schoemaker, Ali A. Mohamoud

TNO, Oude Waalsdorperweg 63, 2597 AK The Hague, The Netherlands

ABSTRACT

This paper aims at the segmentation of seafaring vessels in optical satellite images, which allows an accurate length estimation. In maritime situation awareness, vessel length is an important parameter to classify a vessel. The proposed segmentation system consists of robust foreground-background separation, wake detection and ship-wake separation, simultaneous position and profile clustering and a special module for small vessel segmentation. We compared our system with a baseline implementation on 53 vessels that were observed with GeoEye-1. The results show that the relative L1 error in the length estimation is reduced from 3.9 to 0.5, which is an improvement of 87%. We learned that the wake removal is an important element for the accurate segmentation and length estimation of ships.

Keywords: Satellite images, aerial surveillance, remote sensing, ship recognition, wake removal, multi spectral.

1. INTRODUCTION

Maritime situation awareness is of vital importance in monitoring and control of for instance irregular migration, smuggling, piracy, traffic safety, and fisheries. Monitoring systems that an operator generally has command over are divided in cooperative (e.g. transponder systems such as AIS, VMS and LRIT) and non-cooperative systems (e.g. satellite and airborne observation systems). Cooperative systems are not required for small and non-fishing vessels, can be spoofed, erroneous, or just switched off. In that case an operator falls back on non-cooperative systems, and the vessel length is an important parameter for an operator to classify a vessel. Vessel length is also an important parameter in automatic recognition systems.

Maritime situation awareness is also the area of interest of DOLPHIN, an EU Copernicus research and development project that aims at improving space-based maritime surveillance techniques. Over its 30-month duration, the DOLPHIN project developed new methods and algorithms for processing satellite radar and optical images in order to improve the detection and monitoring of seafaring vessels.

This paper focusses on the segmentation of seafaring vessels in high-resolution optical satellite images, which allows more accurate length estimation. The algorithm consists of robust foreground-background separation, wake detection and ship-wake separation, simultaneous position and profile clustering and a special module for small vessel segmentation. The satellite images are acquired in two modes: multi-spectral (blue, green, red, near-infrared) and panchromatic, in which all the channels are summed to obtain an acceptable signal-to-noise ratio at a higher spatial resolution. We compared our algorithm with a baseline implementation on 53 vessels that were observed with the GeoEye-1 satellite. The results show that the relative L1 error in the length estimates is reduced by 87%. We learned that the wake removal is an important element in the accurate segmentation and length estimation of ships.

The outline of the paper is as follows. The segmentation method is presented in Section 2. The experiments and results are shown in Section 3. Finally, the conclusions and recommendations are presented in Section 4.

[*] henri.bouma@tno.nl; phone +31 888 66 4054; http://www.tno.nl

Henri Bouma, Rob J. Dekker, Robin M. Schoemaker, Ali A. Mohamoud, "Segmentation and wake removal of seafaring vessels in optical satellite images", Proc. SPIE, Vol. 8897, (2013). http://dx.doi.org/10.1117/12.2029791

2. SEGMENTATION METHOD

The main steps in our segmentation method are the following (Figure 1). A robust method is used to estimate the background in order to obtain a reliable initial separation between foreground (ship) and background (water). Unfortunately, the foreground segmentation often includes both ship and wake. Therefore, a separation is made in the foreground object between the two parts based on a simultaneous position and profile clustering. One of these parts is recognized as ship and the other part is removed from the segmentation. Finally, the segmentation of small vessels is improved with a scale-normalized Laplacian and a watershed segmentation. Each of the steps will be described in more detail in the following subsections.

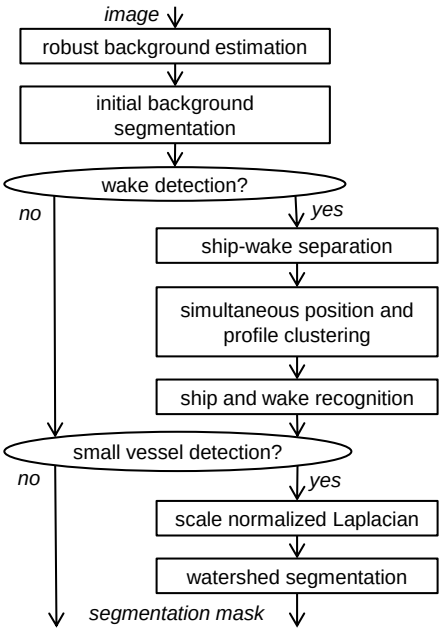

Figure 1: Architecture of the segmentation method.

2.1 Robust estimator in constant time

The first step to obtain an initial foreground-background separation depends on a robust estimation of the background intensity. We propose a novel robust estimator that can be computed in constant time. This estimator is used as input for our initial foreground-background separation to estimate the intensity of the background (i.e. water) independent of the intensity of the foreground object.

Efficient robust estimation is important in the field of computer vision for background estimation, object detection, noise removal, super resolution, filtering, matching and geometry estimation. Average filters or Gaussian filters are often used to regularize the data and to suppress noise. However, these filters are very sensitive to outliers. A median filter already improves the result, but the least median of squares (LMedS or LMS) value [21] gives a robust estimation. There have been several speed optimizations in the computation of LMS [1][2][12][18][19]. Most of the research focused on LMedS as an optimization of multiple parameters in multi-dimensional data. We are now using LMedS as a robust univariate statistic on one-dimensional signals or two-dimensional images.

The following notation is used. We are using square kernels with an odd width k and $n = k^2$ elements, and we define the median as the middle element $(h = floor(n/2))$ of the sorted list.

Bernholt et al. [2] defined the LMedS problem as finding a hyperstrip (i.e. the region between two hyperplanes) such that the half width r of the hyperstrip is minimized. Inspired by this definition, we propose the following fast and exact implementation of the LMedS as a univariate statistic in three steps (see Eq. (1)).

1. $y = \text{sort}(x)$
2. $j = \text{argmin}_i\ (y_{h+i} - y_i)$ (1)
3. $\mu_1 = y_{j+h/2}$; (or according to the LMedS definition the less precise estimate: $\mu_2 = (y_{h+j} + y_j)/2$)

The first step, can be performed on 8-bit integer data or on floating-point data. The sorting of 8-bit integer data of length *n*, can be performed with a non-comparison sort algorithm – such as bucket sort – using 256 bins (or multi-level bins) in linear time *O(n)* [20]. The sorting of floating-point data requires a comparison sort in time *O(n log n)*. The second step is a non-iterative minimization, which is performed in linear time *O(n)* and the third step is performed in constant time. So, the computation of LMedS can be performed in time *O(n)* on 8-bit data, and in time *O(n log n)* on floating-point data.

Perreault et al. [20] proposed a median filtering on 8-bit data in constant time per pixel based on histograms. They proposed a method in three steps. The first step consists of updating the column histogram to the right of the kernel by removing the top pixel and adding the bottom pixel. The second step removes the left column and adds the right column. The last step computes the median. We propose to use the approach of Perreault for the computation of LMedS. The approach can be used to obtain the sorted elements in the kernel and the LMedS value can be computed on the histogram independent of the size of the filter kernel in constant time.

Computing the LMedS as a robust univariate statistic on one-dimensional signals or two-dimensional images, and also the computation of LMedS in constant time, have – to the best of our knowledge – not been presented before. This robust estimate performs much better than the mean or the median for the estimation of the background intensity in the presence of foreground objects, as shown by an example in Appendix A. In the experiments, we used an implementation that was not optimized for speed.

2.2 Initial foreground-background separation

The initial foreground-background separation is applied to the panchromatic image and it consists of the following three steps.

The background intensity is robustly estimated to avoid influences of foreground objects (Sec. 2.1). In our application, the foreground object is usually brighter than the background, especially for larger ships. Therefore, the standard deviation of the water intensity is computed on the pixels p_{dark} that are darker than the robustly estimated background intensity μ_1 (from Sec. 2.1) as:

$$\sigma = \text{sqrt}(\text{mean}((\mu - p_{dark})^2)). \quad (2)$$

The performance of this computation of the standard deviation is shown by an example in Appendix A.

The second step is expectation maximization with a Gaussian mixture model using two Gaussians. The initialization is based on the threshold $thr = \mu_1 + 10\sigma$. Although the factor 10 indicates that the intensity gap between background and foreground is quite large, a separation based on a fixed threshold or a non-robust estimate appeared to be good enough. The mixture model is based on two Gaussians and expectation maximization uses 20 iterations to find an improved separation between foreground and background.

The third step requires the selected object to be close to the center of the detection snippet, because our segmentation is assumed to be applied after a detection step that localizes the seafaring vessel in the center. Furthermore, the largest connected component is selected and morphological opening, closing and hole-filling are performed to remove noise.

2.3 Wake detection and ship-wake separation

The initial segmentation often includes not only a seafaring vessel, but also a wake because it is similar to the ship. Therefore, we perform wake detection and ship-wake separation.

A wake is assumed to be present if either the roundness of the object (= 2π * sqrt(area) / perimeter) is smaller than 0.5, or the segmentation is so large that it is connected to the boundary of the detection snippet (400x400 meter). If the wake is detected, it is removed from the initial segmentation, otherwise the initial segmentation is transferred to the output.

The first step to prepare the ship-wake separation is an estimation of the orientation (principal direction) of the binary mask based on central binary moments.

$$
\begin{aligned}
&x_c = x - E(x);\\
&y_c = y - E(y);\\
&\mu_{11} = E(x_c^{1} * y_c^{1});\\
&\mu_{20} = E(x_c^{2} * y_c^{0});\\
&\mu_{02} = E(x_c^{0} * y_c^{2});\\
&\alpha = \tan^{-1}(2 * \mu_{11} / (\mu_{20} - \mu_{02})) / 2;\\
&\text{if } (\mu_{02} > \mu_{20}),\ \alpha = \alpha + \pi/2;\ \text{end}
\end{aligned}
\tag{3}
$$

where x and y are horizontal and vertical indices, E is the mean value, x_c and y_c are the average indices in horizontal and vertical direction, μ_{xy} is the central moment with the x-order derivative in the horizontal direction and the y-order derivative in the vertical direction, and α is the orientation of the mask.

The orientation α is used to rotate the image so that the length and width of the ships are aligned with the image axes for further analysis.

$$\text{output\_image} = \text{imrotate}(\text{input\_image}, 90 - 180 * \alpha/\pi, \text{'bilinear'}, \text{'crop'}); \tag{4}$$

The width of the segmentation is computed and stored in a vector. The length of the vector is equal to the length N of the segmentation in pixels. The PAN (panchromatic) image is used for the initial segmentation and accurate length measurements because it has the highest resolution, and the BGRN (blue, green, red, near-infrared) image is used for the ship-wake separation because it contains multi-spectral information. To connect information between both, the PAN image is subsampled to obtain the same resolution as the BGRN. Cross-sectional profiles are created in the BGRN image with fixed width W. The profiles of the four BGRN channels are concatenated to create a multi-spectral feature vector of length N and width $4W$. The last step of the ship-wake separation uses this vector and it is based on clustering, which is explained in the next subsection.

2.4 Simultaneous position and profile clustering

The core of the ship-wake separation consists of a clustering method. Clustering is the task of grouping a set of objects in such a way that objects in the same group are more similar to each other than to those in other groups.

Initially, the BGRN feature vector with concatenated cross-sectional profiles was clustered with an ordinary k-means clustering approach [11] to separate the seafaring vessel from the wake. However, this clustering approach is only based on the (dis)similarity of the profiles independent of their position in the segmentation. Therefore, we propose a modified clustering approach to separate vessel and wake that uses simultaneously position and multi-spectral profile similarity information. For each discrete pixel position $(p = [1 : L])$ in the length direction, the ship is separated in two parts on which the average distance to the mean-vector of that part is computed, as in k-means. The location where the two distances are equal gives a split in two parts. An example is shown in Appendix B. This clustering is used to separate the segmentation in two parts, without knowing which part is the ship and which is the wake.

2.5 Ship and wake recognition

Only one of the two parts that is generated by the clustering method contains the ship segmentation and we use our ship and wake recognition module to identify it. Two criteria are used to determine the ship-side and the wake-side of the segmentation. The first is based on the width and the second is based on the brightness.

The width condition is based on the knowledge that the bow is more narrow than the wake and the width of the ship gradually increases from bow towards the center:

$$(W(1) < 0.2 \max(W) \;\&\&\; W(\text{end}) > 0.7 \max(W)) \;||\; (W(1) < 0.4 * \max(W) \;\&\&\; \text{sum}(\text{diff}(W(1:8)) > 0) >= 5) \tag{6}$$

If the condition is true for W, where W is the width-vector, the bow is at the front of the vector. If it is true for W, where W is the reverse of the width vector, the bow is at the back of the vector. If both are true or none is true then the

brightness condition is used to determine the front. The brightest side is determined as the maximum intensity of the near-infrared channel. If the separation leads to smaller fragments, then only the largest connected component is identified as ship.

2.6 Segmentation of small sea-faring vessels

The small vessels require a slightly different approach than the other objects. This consists of two steps: scale-normalized Laplacian and watershed segmentation.

Detection of small vessels is based on the length of the segmentation that is received as input. If the length of the ship is smaller than 10 meter it is considered as a small vessel.

Small ships are similar to blobs. A common approach to detect blobs is the Laplacian, which is based on Gaussian derivatives [4].

$$\Delta L = L_{xx} + L_{yy} \tag{7}$$

However, the main problem of the Laplacian as blob detector is that it only responds to blobs at one scale. Therefore, a scale-normalized Laplacian [17] was used to detect small vessels, where the maximum response is related to the best scale.

$$\Delta N = \sigma^2 \cdot \Delta L \tag{8}$$

The scale-normalized Lapacian gives an optimal response to blobs of the related size. This is used as input for the watershed segmentation. The segmentation of small vessels is based on hysteresis thresholding where the boundaries of the watershed are removed in the segmentation of the lower threshold and where the segmentation of the high response of the Laplacian is used as seed.

3. EXPERIMENTS AND RESULTS

3.1 Data set with image snippets

For our experiment, we used images that are acquired by the GeoEye-1 satellite, which is an earth observation satellite owned by the commercial company GeoEye Inc. The data consists of four BGRN channels (blue, green, red, near-infrared) and one PAN (panchromatic) channel. Spatial resolution of the BGRN channels is 2.0m, and that of the PAN image is 0.5m. Detections were generated manually, resulting in snippets of 400x400 meters with the target approximately in the center of the image. The BGRN image snippets have a lower resolution (200x200 pixels) and the PAN image snippets have a higher resolution (800x800 pixels). Initially, 80 snippets were selected. Of these images, 27 were removed because they contained ships in the harbor or airplanes. The segmentation results are based on 40 seafaring vessels and 13 buoys in open sea (Table 1). Ground-truth of the larger vessels (> 300m) was obtained from in-situ AIS (Automatic Identification System) data. Ground truth of the smaller vessels and buoys not transmitting AIS was obtained by visual inspection of the panchromatic image. Examples of the used RGB and panchromatic snippets are shown in Figure 2.

Table 1: The number of snippets used for segmentation in the optical satellite images and the average ground-truth length and width (av ± std).

Vessel type	nr of image imagettes	GT length (meter)	GT width (meter)
Tanker	5	181 ± 64	29 ± 10
Dredger	6	115 ± 32	22 ± 5
Cargo	1	120	15
Tug	1	26	11
Sailing vessel	2	20 ± 5	7 ± 1
Fishing	4	16 ± 7	5 ± 1
Buoy	13	3 ± 0	3 ± 0
Unknown	15	27 ± 30	6 ± 3
Other	7	86 ± 82	20 ± 18

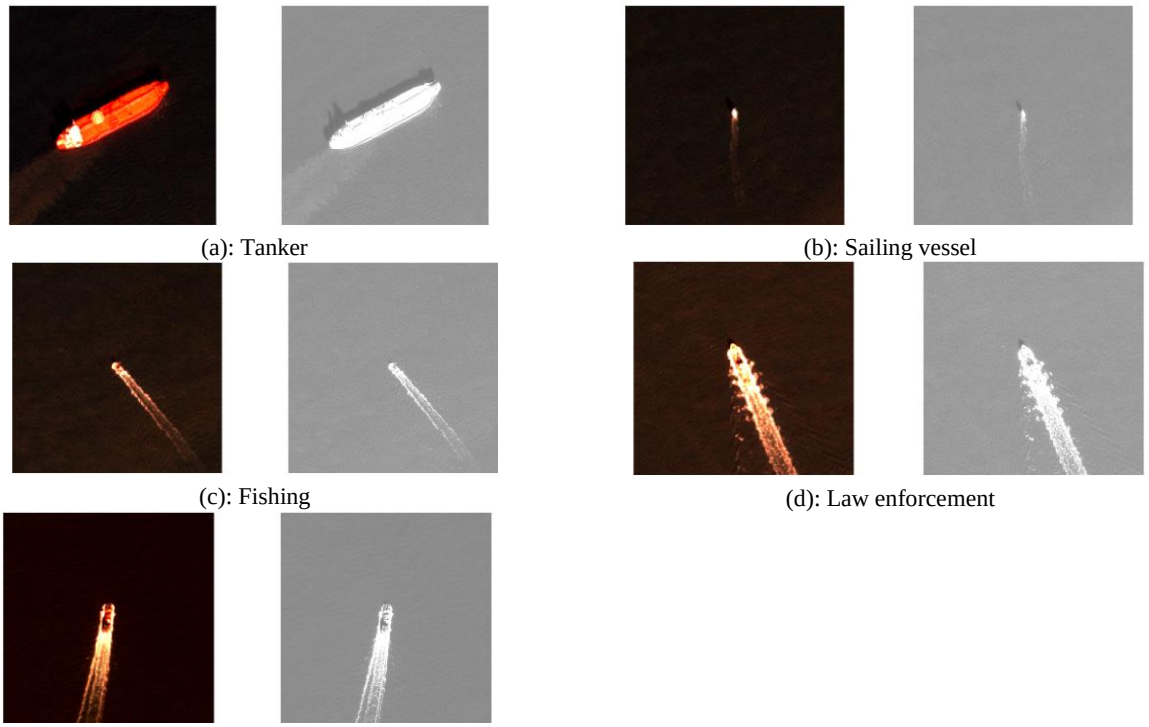

(a): Tanker (b): Sailing vessel

(c): Fishing (d): Law enforcement

(e): Anti-pollution

Figure 2: Examples of RGB and Panchromatic snippets. © GeoEye Inc. (2011), provided by e-GEOS S.p.A. under GSC-DA.

3.2 Segmentation results

The ships are segmented with the proposed method and a few segmentation examples are shown in Figure 3.

The absolute (9) and relative (10) errors are computed:

$$err_{abs} = (L_{est} - L_{gt}) \quad (9)$$

$$err_{rel} = (L_{est} - L_{gt}) / L_{gt} \quad (10)$$

The absolute and relative results are shown in Figure 4 and Figure 5 respectively for each vessel. The total error is computed as the L_1 and the L_2 norm (Eq. 11 and 12 resp.) and shown in Table 2.

$$L_1 = \text{mean}(\text{abs}(err)) \quad (11)$$

$L_2 = \text{sqrt}(\text{mean}(\text{err}^2))$ (12)

(a): Tanker

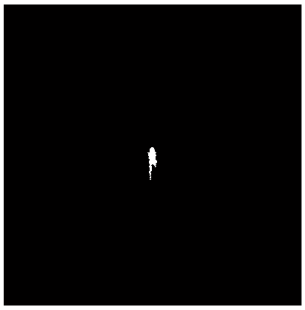

(b): Sailing vessel

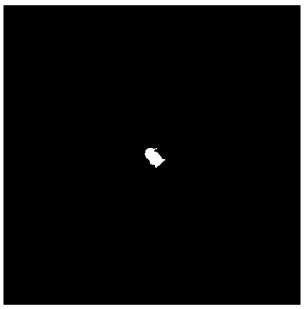

(c): Fishing

(d): Law enforcement

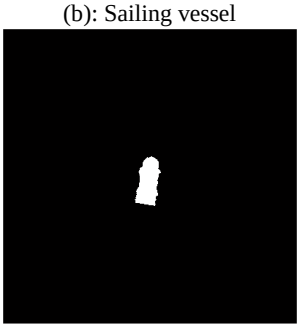

(e): Anti-pollution

Figure 3: Examples of segmentations of the snippets.

Table 2: Correlation, L1 and L2 error of absolute length and relative errors. The proposed system is also compared with the initial segmentation of Sec. 2.1 and 2.2. Produced using products © GeoEye Inc. (2011), provided by e-GEOS S.p.A. GSC-DA.

Error type	**Error measure**	**Initial segm.**	**Proposed system**
Correlation	correlation(Lest, Lgt)	0.67	0.93 (+39%)
Absolute L1 error	mean(abs(Lest – Lgt))	51.2	12.8 (-75%)
Absolute L2 error	sqrt(mean((Lest – Lgt)^2))	87.7	25.9 (-70%)
Relative L1 error	mean(abs((Lest – Lgt)/Lgt))	3.90	0.51 (-87%)
Relative L2 error	sqrt(mean(((Lest – Lgt)/Lgt)^2))	2.18	0.93 (-57%)

Table 2 shows the errors of the initial segmentation (Sec. 2.1 and 2.2) and the proposed system. The results show that the relative L1 error in the length estimation is reduced from 3.90 to 0.51, which is an improvement of 87%. The main difference between the initial segmentation and the proposed system is the wake removal. This appears to be an important element for the accurate segmentation and length estimation of ships.

The current approach assumes that the wake is a straight structure behind the ship, which is invalid when the ship is maneuvering or in cases of strong side wind. Further development of these aspects would require more satellite images.

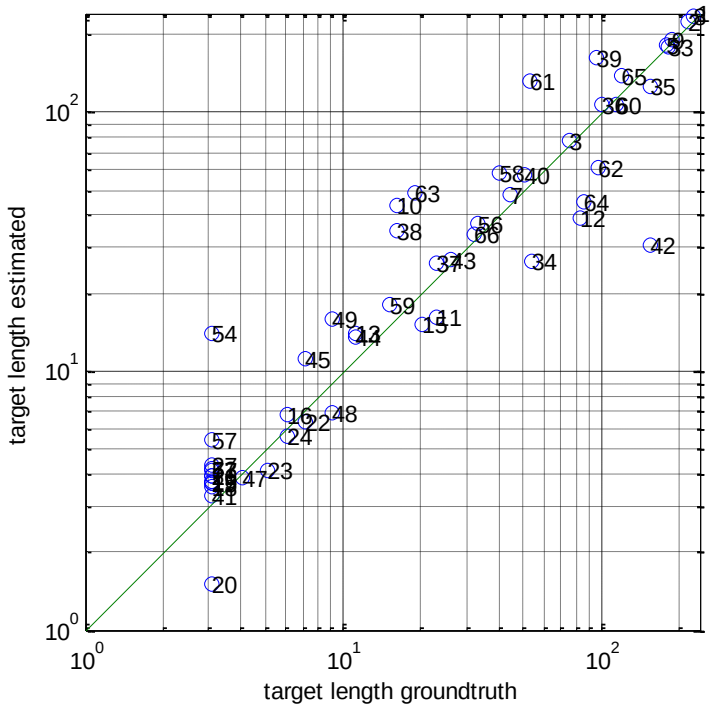

Figure 4: True versus estimated target length on a logarithmic scale.

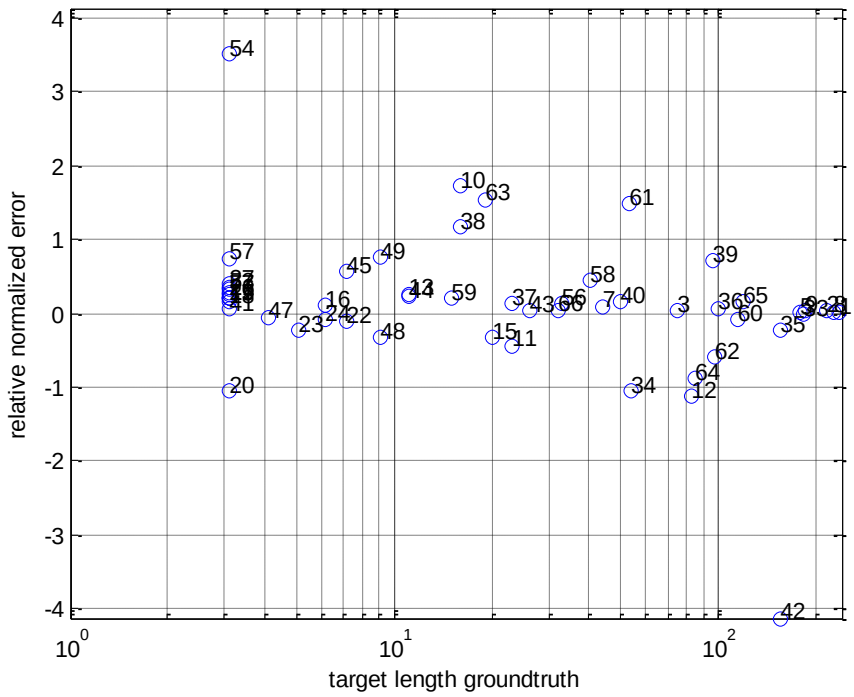

Figure 5: True target length versus relative error *(Lest - Lgt)/Lgt*.

4. CONCLUSIONS

This paper focused on the segmentation of seafaring vessels in optical satellite images, which allows more accurate length estimation. The system consists of robust foreground-background separation, wake detection and ship-wake separation, simultaneous position and profile clustering and a special module for small vessel segmentation. We compared our system with a baseline implementation on 54 vessels that were observed with GeoEye-1. The results show that the relative L1 error in the length estimation is reduced from 3.9 to 0.5, which is an improvement of 87%. We learned that the wake removal is an important element for the accurate segmentation and length estimation of ships. Further development would require more satellite data.

APPENDIX A: ROBUST ESTIMATION EXAMPLE

For background-foreground separation it is important to accurately estimate the parameters of the dominant background distribution and separate it from the foreground object. This appendix shows an example of the robust estimator (Eq. 1), the standard deviation (Eq. 2) and expectation maximization with a Gaussian mixture model on artificial data. Two Gaussian (normal) distributions are used for illustration purposes. The first distribution consists of a mean μ_1=1.0, standard deviation σ_1=1.0 and N_1=10000 samples, and the second distribution consists of μ_2=5.0, σ_2=1.0 and N_2=5000 (see Figure 6). The first distribution is dominant because $N_1 > N_2$.

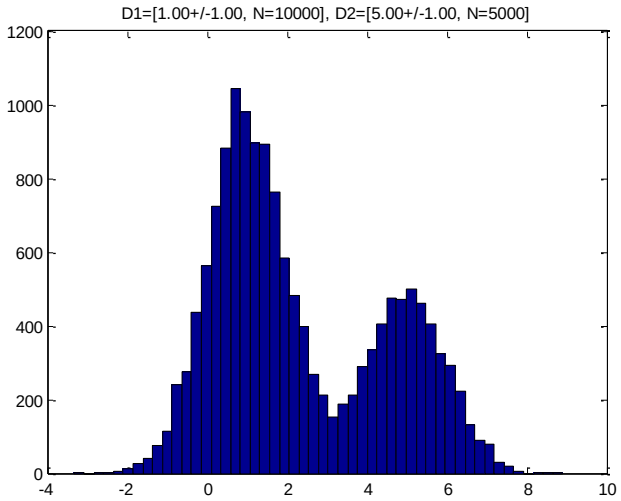

Figure 6: Two Gaussian distributions (μ_1=1.0, σ_1=1.0, N_1=10000 and μ_2=5.0, σ_2=1.0, N_2=5000).

In order to estimate the mean of the dominant distribution (μ_1), we compared the average, median and the robust estimator (Eq. 1) and for the estimation of the standard deviation (σ_1) of this distribution, we compared the ordinary standard deviation and the estimate over the lower part (Eq. 2). The results are based on 20 iterations and they are shown in Table 3. The table shows that Eq. (1) and Eq. (2) give accurate estimates of parameters of the dominant distribution. The robust estimator proves to be much more accurate than the average or the median.

Table 3: Estimates of the mean (μ_1) and the standard deviation (σ_1) of the dominant distribution and a separation between the two distributions. The table shows that Eq. 1 and 2 give robust estimates of the dominant distribution.

Error measure	Estimate	Error
Average	2.33 ± 0.01	1.33 ± 0.01
Median	1.68 ± 0.01	0.68 ± 0.01
Robust estimator: Eq. (1)	1.00 ± 0.03	**0.00** ± 0.03
Standard deviation over all samples	2.13 ± 0.01	1.13 ± 0.01
Standard deviation over lower part: Eq. (2)	1.00 ± 0.02	**0.00** ± 0.02
EM + GMM initiated at $\mu_1 + 0\sigma_1$	3.22 ± 0.03	0.04 ± 0.03
EM + GMM initiated at $\mu_1 + 4\sigma_1$	3.24 ± 0.03	0.06 ± 0.03

APPENDIX B: CLUSTERING EXAMPLE

This appendix shows a one-dimensional clustering example on artificial data. Figure 7 illustrates the difference between ordinary k-means clustering and the simultaneous position and profile clustering. The key part in this clustering is the computation of the cluster distance (Figure 7c). The blue (rising) distance curve shows for each pixel *p*, the average distance of all pixels in the range *[1:p]* to the mean over that range. The green (falling) curve shows for each pixel *p*, the average distance of all pixels in the range *[p:end]* to the mean over that range. The figure shows that the proposed approach gives a more robust indication of the separation in two parts than k-means clustering.

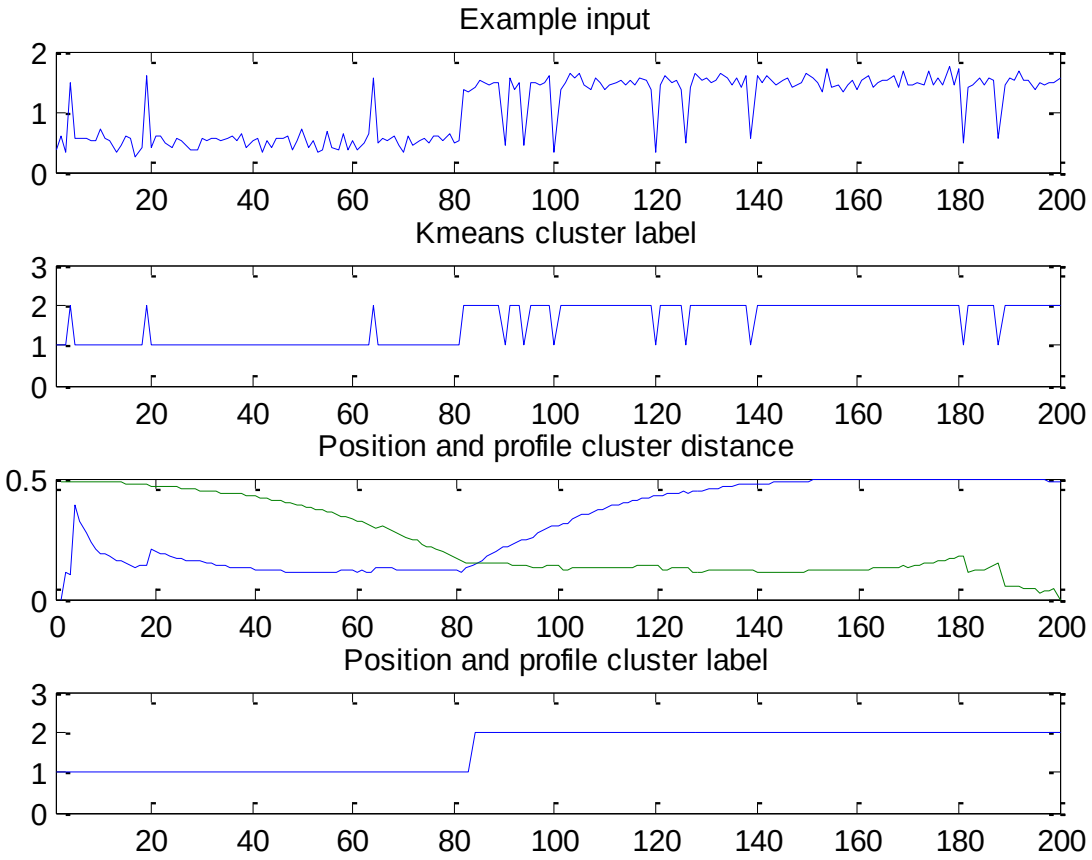

Figure 7: One-dimensional example of the position and profile clustering. The figure shows (a) the example input is a noisy signal, (b) the k-means cluster labels, (c) the simultaneous position and profile cluster distance and (d) the position and profile cluster labels.

ACKNOWLEDGEMENT

The research leading to these results has received funding from the European Union Seventh Framework Programme (FP7/2007-2013) under the DOLPHIN project, grant agreement no. 263079. DOLPHIN is part of the European Earth Observation Programme Copernicus, previously known as GMES (Global Monitoring for Environment and Security). Additional funding was received from the Netherlands MoD program V1114, Maritime Situational Awareness.

REFERENCES

[1] Agullo, J., "Exact algorithms for computing the least median of squares estimate in multiple linear regression algorithm," IMS Lecture Notes Monograph Series 31, 133 – 146 (1997).
[2] Bernholt, T., "Computing the least median of squares estimator in time O(nd)," Computational Science and its Applications LNCS 3480, 697 – 706 (2005).
[3] Bouma, H., Lange, D.J. de, Broek, S.P. van den, Kemp, R., Schwering, P., "Automatic detection of small surface targets with electro-optical sensors in a harbor environment," Proc. SPIE 7114, (2008).
[4] Bouma, H., Vilanova, A., Olivan Bescos, J., Haar Romeny, B.M. ter, Gerritsen, F.A., "Fast and accurate Gaussian derivatives based on B-splines," Proc. Scale space and variational methods LNCS 4485, (2007).
[5] Broek, B. van den, Breejen, E. den, Dekker, R., Smith, A, "Change detection and maritime situation awareness in the channel area - Feasibility of space borne SAR for maritime situation awareness," IEEE Int. Geoscience and Remote Sensing Symp., 7436 – 7439 (2012).
[6] Broek, S.P. van den, Schwering, P., Liem, K., Schleijpen, R., "Persistent maritime surveillance using multi-sensor feature association and classification," Proc. SPIE 8392, (2012).
[7] Broek, S.P. van den, Bouma, H., Degache, M., "Discriminating small extended targets at sea from clutter and other classes of boats in infrared and visual light imagery," Proc. SPIE 6969, (2008).
[8] Broek, S.P. van den, Bouma, H., Degache, M., Burghouts, G., "Discrimination of classes of ships for aided recognition in a coastal environment," Proc. SPIE 7335, (2009).
[9] Daniel, B., Schaum, A., Allman, E., Leathers, R., Downes, T., "Automatic ship detection from commercial multispectral satellite imagery," Proc. SPIE 8743, (2013).
[10] Dekker, R., Bouma, H., Breejen, E. den, Broek, B. van den, Hanckmann, P., Hogervorst, M., Mohamoud, A., Schoemaker, R., Sijs, J., Tan, R., Toet, A., Smith, A., "Maritime situation awareness capabilities from satellite and terrestrial sensor systems," Proc. Maritime Systems and Technologies MAST Europe, (2013).
[11] Duin, R.P.W., Juszczak, P., Paclik, P., Pekalska, E., de Ridder, D., Tax, D.M.J., "PRTools4: A Matlab toolbox for pattern recognition," Delft University of Technology, (2004).
[12] Erickson, J., Har-Peled, S., Mount, D.M., "On the least median square problem," Discrete and Computational Geometry 36(4), 593 – 607 (2006).
[13] Gil, J., Werman, M., "Computing 2-dimensional min, median and max filters," IEEE T. Pattern Analysis and Machine Intelligence 15(5), 504 – 507 (1993).
[14] Johansson, P., "Small vessel detection in high quality optical satellite imagery," Tech. Report Chalmers University of Technology Sweden, (2011).
[15] Joslin, E., "Method for automatically fusing IMINT with AIS," Tech. Report SPAWAR USA, (2012).
[16] Kumar, S.S., Selvi, M.U., "Sea object detection using colour and texture classification," Int. J. Computer Appl. in Engineering Sciences IJCAES 1(1), 59-63 (2011).
[17] Lindeberg, T., "Feature detection with automatic scale selection," Int. J. Computer Vision 30 (2), (1998).
[18] Mount, D.M., Netanyahu, N.S., Romanik, K., Silverman, R., Wu, A.Y., "A practical approximation algorithm for the LMS line estimator," Computational Statistics and Data Analysis 51(5), 2461–2486 (2007).
[19] Olson, C.F., "An approximation algorithm for least median of squares regression," Information Processing Letters 63(5), 237–241 (1997).
[20] Perreault, S., Hebert, P., "Median filtering in constant time," IEEE T. Image Processing 16(9), 2389–2394 (2007).
[21] Rousseeuw, P.J., "Least median of squares regression," J. American Statistical Association 79, 871 – 880 (1984).
[22] Withagen, P., Schutte, K., Vossepoel, A., Breuers, M., "Automatic classification of ships from infrared (FLIR) images," Proc. SPIE 3720, (1999).